

# AERODYNAMIC ANALYSIS OF TILTROTORS IN HOVERING AND PROPELLER MODES USING ADVANCED NAVIER-STOKES COMPUTATIONS

S. Gates<sup>1</sup>

AgustaWestland, Yeovil, UK

Existing helicopter aerodynamic design and analysis tools require adaption and validation for tiltrotor configurations before they can be used by industry. In this paper, the application of a Computational Fluid Dynamics tool to an isolated tiltrotor is presented as an example of the on-going development work in AgustaWestland. Simulations for hovering and propeller cases have been performed and compared with published experimental data and a good agreement has been found. The discussion includes the application of an overset mesh approach.

## NOMENCLATURE

$AoA$	Aerofoil Angle-of-Attack [°]
$c$	Reference chord [m]
$CFD$	Computational Fluid Dynamics
$C_p$	Pressure coefficient [ ]
$C_Q$	Rotor torque coefficient [ ]
$C_T$	Rotor thrust coefficient [ ]
$FoM$	Rotor Figure of merit [ ]
$M_{tip}$	Rotor tip Mach number [ ]
$p$	Static pressure [Pa]
$Q$	Rotor torque [Nm] or ‘Q Criterion’
$R$	Radial distance from rotor shaft axis [m]
$R$	Rotor tip radius [m]
$Re$	Tip Reynolds number [ ]
$T$	Rotor thrust [N]
$\theta_{75}$	Collective at 75%R [°]
$\eta$	Propulsive efficiency, $(C_T \times advance\ ratio)/C_Q$ [ ]

## 1 INTRODUCTION

Significant interest exists in combining the helicopter’s vertical take-off/landing capability with the high speed and range capabilities of turbo-prop aircraft. AgustaWestland is leading the pursuit of this goal through the development and certification of the AW609 tiltrotor.

In order to progress tiltrotor technology and improve performance, aerodynamic analysis tools must be developed which are capable of providing accurate, reliable performance data

for these rotor types. Since they must operate in propeller mode, tiltrotors differ from helicopter main rotors in that their blades are highly twisted, have thicker root sections and due to radius constraints must operate at higher hover disk loadings. Therefore, existing helicopter aerodynamic design and analysis tools must first be adapted and validated for such unconventional rotor configurations before they can be used by industry.

HMB 2.0 is a Computational Fluid Dynamics (CFD) developed at the University of Liverpool, home of the AgustaWestland Liverpool Advanced Rotorcraft Centre (AWLARC), [1]. It is routinely used within AgustaWestland Aerodynamics to assist in research, analysis and the design of aerofoil sections and helicopter rotors amongst other day-to-day aerodynamics tasks. In support of AgustaWestland product development, the tool has recently been applied and tested on various tiltrotor configurations. An example case is presented here to explain how the developed methodology is being used. Comparisons with published experimental data will be used to demonstrate the validity of the computational approach. This paper is divided into three sections; hover results, computations for propeller mode and finally comparisons

---

<sup>1</sup>HSD-Aerodynamics,  
stuart.gates@agustawestland.com

between Chimera and baseline mesh flow solutions.

## 2 XV-15

The XV-15 is a tiltrotor aircraft developed jointly by Bell and NASA which first flew in the 1970s (Figure 1). The aircraft was a forerunner to the Bell-Boeing V-22 Osprey and AW609 tiltrotors which owe much of their basic technology to the development and research work performed during the XV-15 project [2].

Based upon information available in the published literature, the rotor geometry has been created for use as an HMB test case. The blade twist and chord distributions were published in [3] and are shown in Figure 2 for reference. The identity and radial location of the blade aerofoil sections are detailed in [4] and listed in Table 1. The NACA 6-series sections have been generated using the procedure described in [5]. It is expected that this method provides at least a reasonable approximation of the manufactured shapes. The inboard blade stations have been neglected due to the unavailability of the true cuff geometry in the public domain. The blade 3D surfaces were generated using CATIA<sup>®</sup> v5 and the resulting rotor surface geometry is shown in Figure 3. A representative trailing edge tab thickness along the length of the blade has been introduced for realism.

## 3 HOVER

### 3.1 Hover Mesh

The isolated rotor in hover/axial-flight is approximated as a steady-state problem and only 1blade is meshed with the flow treated as a periodic in space and time [1]. Fully-structured multi-block hexa meshes are generated using ANSYS<sup>®</sup> software. The baseline hover mesh was constructed for  $\theta_{75}=10^\circ$ . HMB includes a utility to trim grids which allows the user to obtain a range of collective pitch settings from the baseline mesh. Although flap angles can also be inserted, in the present work coning has been neglected since it is expected to have little impact on the results for small angles. A modified sliding plane [6] boundary condition is used at the periodic plane in the hover mesh to

accommodate a non-conformal blocking-topology which has been chosen to suit the blunt trailing edge geometry of the blades.

A cylindrical hub of 5%R separates the periodic planes. A first near-wall cell height of  $1\times 10^{-5}c$  provides a satisfactory compromise between the resolution of the boundary layer flow gradients and limiting the total mesh size. The total mesh size is approximately 10million cells.

One difficulty with the CFD simulation of hovering rotors is the prescription of the domain far field boundary conditions. If their specification is based upon the quiescent flow outside of the mesh domain, then the flow in/out of the domain is near-zero. The result of this specification is equivalent to placing the rotor inside a closed box and typically leads to flow recirculation and ingestion by the rotor. It is for this reason experimental hover tests must be performed in very large indoor spaces, clear of obstructions. Lacking guidance, the initial solution is often incorrect and can be difficult or impossible to recover from. Rather than increasing the mesh domain at the expense of additional cells and computing resources, an efficient alternative, proposed by Srinivasan et al. [7], is to place a three-dimensional point sink of a magnitude which corresponds with the expected rotor thrust at the rotor centre. The sink attracts flow into the CFD domain from outside. In order to respect the conservation law, this inflow must be balanced by an outflow. This is prescribed on the outlet boundary surface and is based upon momentum theory using the same expected rotor thrust value. The flow velocity magnitudes near the boundary are very small in comparison with the rotor wake, and it is the direction which assists in establishing a realistic hover wake solution. This boundary configuration has been used to promote the stable hovering rotor solutions presented here and insensitivity in terms of wake geometry and forces prediction has been confirmed.

### 3.2 Hover Simulations

HMB hover simulations were performed for the conditions in Table 2 to produce a polar of results at various  $\theta_{75}$ . The  $k-\omega$  SST turbulence model was used for all results reported in this paper [8].

All presented simulations were obtained using in-house AgustaWestland High-Performance Computing (HPC) facilities.

All simulations were continued until solution residuals dropped at least 4 orders of magnitude and steady converged force outputs were observed. An example of a hover simulation convergence history is provided in Figure 5. The history of the sensitive FoM parameter provides a strong indication that a steady solution has been found.

### 3.3 Hover Rotor Wake Predictions

A selection of the computed rotor wakes are shown in Figure 6 using the Q-criterion method for vortex identification, [9] (Note that the 1-blade periodic simulations have been rotated to re-create the 3-bladed flow field). The roll-up of the vortex around the blade tip is visible. The simulations predict the path of the tip vortices as they are trailed behind the blade.

The trailed tip vortices pass close to the following blade at  $\theta_{75} = 6$  and  $10^\circ$ . Wake contraction appears rapid and is attributed to the high disk loading compared with a conventional helicopter main rotor. The wake can be seen to be preserved beyond the first blade passage at the chosen Q-level. Modelling of the first passage is crucial in ensuring a realistic prediction of the wake-induced effects on the blade loading, whilst the second has lesser importance but still interacts with the first. In all simulations a large root vortex is predicted due to the roll-up around the thick root cut out aerofoil section which is certainly different from the real aircraft where the blade is attached to the hub. The effect of this geometry simplification has been investigated for various other rotor configurations, not presented here. In the case of the  $\theta_{75}=3^\circ$  simulation the vorticity was more difficult to trace and may be explained by the extremely close passage or

even a direct impact of the trailed vortex path with the following blade.

### 3.4 Hover Surface Pressure Predictions

Figure 7 presents the predicted pressure coefficient contours for the blade upper surfaces (with  $C_{plocal}$  based upon local dynamic pressure). The results show the loading distributions which have been achieved with this highly twisted rotor design. The thick inboard sections appear loaded and the roll-up of an artificial root vortex is evident, however the contribution of these features is diminished by the low local dynamic head. At  $\theta_{75}=10$  and  $13^\circ$  the distributions at outboard blade stations show a strong suction peak which exceeds the critical value.

Experimental surface pressure measurements were not available; however the predicted chordwise pressure distributions have been compared with the sectional CFD data published by Kaul & Ahmad in [10]. Their results were obtained using the OVERFLOW2 flow solver, 35million+ cells and the Spalart Allmaras (SA) turbulence model compared with the 10million cells and  $k-\omega$  SST model used in the HMB simulations. The agreement between the numerical predictions is impressive considering the smaller mesh size used in HMB and the potential for numerical dissipation of the rotor wake in the fully-turbulent solution. Some variation is to be expected due to the geometric approximations. The data extracted at the 94%R radial station confirms the suction peak has exceeded the critical  $C_p$  value. The growth of the supercritical region is more clearly visible in Figure 9. The region was found to extend further along the blade span with increasing incidence compared with conventional helicopter main rotors. Figure 10 presents the HMB surface streamline predictions for  $\theta_{75}=10$  and  $13^\circ$ . At  $\theta_{75}=10^\circ$ , within the normal operating range of the rotor, the flow remains attached confirming a good selection of rotor twist and aerofoil sections in this blade design. At  $\theta_{75}=13^\circ$  the shock feature is evident, but the downstream flow is predicted to remain attached. The additional incidence has pushed

the aerofoil sections close to their limits and eventually shock-induced separations and drag divergence will result. The separation location is determined by the close passage of the preceding blade's trailed tip vortex; the local upwash from the outboard side of the vortex acts to increase the local  $AoA$  experienced by the aerofoil sections, resulting in separated flow. Also evident in the figure is the roll-up of tip vortex around the rectangular-shaped tip – the evidence of induced drag.

### 3.5 Hover Radial Loading Distributions

The predicted chordwise surface pressure distributions have been integrated to obtain the distribution of loading and torque along the blade radius (Figure 11 and 12). The high twist has helped the blade achieve a reasonably 'uniform' loading distribution. The influence of the passing trailed tip-vortex is visible as the spikes in loading around 92%R. The predicted torque distributions indicate the corresponding power divergence.

### 3.6 Hover Integrated Loads vs. Experiment

As previously summarised by Betzina in [11], several sets of NASA experimental measurements are available for comparison which were collected using the Outdoor Aerodynamic Research Facility (OARF, [4]) and 80x120ft wind tunnel [11],[12]. All datasets are for the full-scale XV-15 rotor and have been corrected for hub and apparatus tares making them suitable for comparison with isolated rotor simulations. The agreement between the HMB total force predictions and test measurements is excellent throughout the range of collective pitch angles studied (Figure 13 and 14). The trend and values of the sensitive FoM parameter have been captured from a low thrust condition, through the peak value and up to very demanding conditions, where the steady approximation will cease to be valid and power divergence occurs. This validation confirms the suitability of the methodology for tiltrotor blade applications. The obtained agreement is an indication that the

CFD model is sufficiently capturing the induced-effects of the rotor wake and that the chosen  $k-\omega$  SST turbulence model provides a good approximation of the near-wall effects. The HMB data reported are the raw output from the code, without need for modification or corrections. The HMB integrated loads data is provided in Table 4.

The predicted peak FoM is high and indicates good rotor hover performance, approaching the maximum possible with conventional rotor technology. The apparent impressive performance owes a lot to the high disk loading operating range and use of a high blade twist (not possible on conventional helicopter main rotors), but also confirms a good selection and placement of aerofoil sections.

## 4 PROPELLER SIMULATIONS

### 4.1 Propeller Mesh

As with the hover simulations, the isolated propeller (axial flight) mode cases are modelled as steady-state periodic problems. Two propeller meshes have been generated – one with a moderate pitch setting and a second with a low collective pitch. Used in combination with the HMB grid trimming tool, these two meshes are sufficient to cover a wide range of pitch settings. The blocking topology used in the propeller mesh was developed from the hover mesh with a 90° rotation about the x-axis and is fully-conformal at the periodic boundary. Modifications were made at the hub to include the hub spinner. The total mesh size is maintained as 10million cells.

### 4.2 Propeller Simulations

Simulation configuration and execution for the HMB propeller cases is very similar to the approach described for the hover cases. Simulations were performed for low and moderate advance ratios at the conditions shown in Table 3. The propeller simulations were found to converge rapidly to steady solutions. The downstream convection of the rotor wake in propeller mode reduces its interaction with the

following blades, resulting in a much less-complex and more easily-established flow problem to solve compared with the hovering rotor and consequently reduced run-times.

### 4.3 Propeller Rotor Wake Predictions

Figure 16 shows the HMB propeller wake predictions for the two advance ratios studied using the Q-criterion [9]. Many revolutions of rotor wake are preserved in each of the cases, and only ended as shown due to the termination of the calculations - when the residuals indicated converged solutions and the integrated forces on the blade had settled to steady values, the simulations were halted. After the first revolution, the shape and size of the vortex can be seen to suffer some deformation which is due to the convection into progressively coarser regions of the mesh. Although not an issue for the present work in predicting the isolated rotor performance, if a rotor wake-fuselage interactional problem were requested, the mesh could be refined to better preserve the trailed propeller wake far downstream of the rotor disk.

### 4.4 Propeller Surface Pressure Predictions

Figure 17 and 18 present the predicted pressure coefficient contours for the blade upper and lower surfaces at the two simulated advance ratios (with  $C_{plocal}$  based upon local dynamic pressure). At low  $C_T$  the results indicate some loading on the inboard end of the lower surface which is acting in the opposite direction to the rotor thrust. As the collective is increased into the normal operating range this feature reduces somewhat and the contours indicate the loading is reasonably distributed along the blade upper surface.

### 4.5 Propeller Radial Loading Distributions

The surface pressure distributions have been integrated to obtain radial loading and torque distributions for the various conditions, Figure 19 and 20. The local quantities reported are scaled in the same way as the hover plots for consistency. As noticed in the surface pressure contours, the predicted inboard loadings on the

prop-rotor are negative and indicate a ‘braking’ effect on the aircraft with corresponding power absorption up to 60%R, dependant on the advance ratio and the pitch-setting.

### 4.6 Propeller Integrated Loads vs. Experiment

The HMB total loads predictions are compared with the propeller test data reported in [13]-[15] in Figure 21. The HMB isolated rotor predictions (red curves) provide a good match to the measured data at both the low and moderate advance ratio conditions simulated. The variation at the lowest  $C_T$  points is attributed to the missing root end geometry in the simulations – referring again to the radial loading distributions presented earlier (Figure 19 & Figure 20), it would be reasonable to expect that if the blade root cuff geometry had been included in the simulations, they would carry an additional negative thrust contribution, and particularly at low  $C_T$ . These additional negative contributions would reduce the net rotor thrust, to a greater extent in the moderate advance ratio case, which would improve the agreement reported in Figure 21.

Since the spinner loads data is available from the HMB simulations, a separate (green) curve is inserted to report the predicted ‘net’ rotor thrust and highlight the significant role the spinner component plays in the overall prop rotor performance. The drag of the spinner effectively reduces the rotor  $C_T$  and this is evident in the presented data. It is clear that in order to design an efficient propeller, the spinner design is an important aspect of the process. The HMB propeller data is provided in Table 5.

In Figure 22 the HMB predictions are compared with the test scatter points published in [16] where the authors assert that since the data was collected well below the drag divergence Mach number, there is little sensitivity to the advance ratio or the  $M_{TIP}$  at which each test point was recorded. The HMB predictions appear to agree with this claim; the simulation data for both advance ratios lying within the test scatter. Once again, the variation

at the lowest  $C_T$  is attributed to the absence of the blade root sections from the simulations.

Although the agreement between the HMB propeller predictions and the measurements is good, it should be expected – the convection of the rotor wake downstream of the disk makes the propeller simulation ‘straightforward’ in comparison with the hover case and much simpler numerical methods are capable of providing good performance predictions. Nevertheless, the validation exercise is necessary prior to the use of a tool by industry for design or aircraft performance work and the additional detailed design information which can be obtained from the CFD simulations justifies the effort.

Despite the reverse thrust identified on inboard stations – which could possibly be eliminated by a twist or aerofoil refinement – an efficient propeller design is evident, especially considering that any prop-rotor design must also satisfy the requirements of the hover case, operating with a higher disk area and lower blade loading than might be desirable.

## 5 CHIMERA COMPARISON

Recently an overset, ‘Chimera’ mesh capability has been added to HMB, [17]. A repeat of the XV-15 hover analysis for  $\theta_{75}=10^\circ$  will be presented to demonstrate the functionality of the new approach.

### 5.1 Chimera Mesh

The Chimera mesh domain and near-blade blocking topology are shown in Figure 23. A foreground mesh was constructed for the region close to the rotor blade. This mesh is similar to the original hover mesh, but the removal of the conformity constraints at the boundary allows for minor quality improvements and the addition of more cells without significant impact on the total mesh size. The separate background mesh, which fills the entire  $\psi=120^\circ$  wedge volume, is essentially a Cartesian mesh and is therefore of high-quality. The decoupling of the near and far mesh domains allows more flexibility in the placement of cells and

concentrations have been located to resolve the trailed tip vortex wake. The total mesh size was constrained to be the same size as the original hover mesh in order to provide a fair comparison between the two simulations (10million cells).

### 5.2 Chimera Simulations

The HMB Chimera implementation uses a 2<sup>nd</sup> order interpolation between the mesh levels. Solution run-times demonstrated no noticeable overhead for the additional calculations and considering the simplified mesh generation task, the overall time to complete the simulation task was reduced.

### 5.3 Chimera Rotor Wake Predictions

The computed wake prediction shows many revolutions of rotor wake have been preserved in the HMB Chimera simulation. The improved resolution of the tip vortex due to the finer concentration and regularity in cell placement is evident. Numerical dissipation due to coarse mesh regions or poor cell quality has been delayed far downstream of the region of interest. Comparing with the wakes predicted using the baseline hover mesh (Figure 6), the tip vortex is not only traced for longer, but maintains its form (and energy) without bursting and as a result the full wake contraction and classic streamtube shape is visible.

### 5.4 Chimera Surface Pressure Predictions

Figure 25 compares the predicted surface pressure distributions obtained with the Chimera mesh with those reported using the baseline mesh. There is a very close agreement between the two predictions, giving confidence in the new methodology. The minimal variations are attributable to the variation in the capture of the induced effects of the 1<sup>st</sup> passing trailed vortex.

### 5.5 Chimera Radial Loading Distributions

The obtained radial loading and torque distributions for the Chimera simulation are presented in Figure 26. The distributions show

a very close agreement with those extracted from the baseline mesh simulation. Upon close inspection it can be seen that the Chimera mesh result has better-captured the induced effects of the passing tip vortex – causing a slightly deeper local drop in loading at 84%R and higher peak at 92%R.

### 5.6 Chimera Integrated Loads vs. Baseline Results and Experiment

The HMB Chimera total force results are shown to be in excellent agreement with the original hover data in Table 6. The Chimera prediction for the sensitive FoM parameter is within 0.3% of the baseline mesh  $\theta_{75}=10^\circ$  result. The results are compared with the experimental data from [11] in Figure 27 to confirm that the variation is very small and the results both lie within the hover test measurement point scatter. In addition to verifying the implementation of the Chimera method in HMB, this result provides some evidence of the mesh-independence of the baseline solution.

Further validation work is required, but the addition of Chimera to the HMB toolset is envisaged to greatly assist in the meshing and simulation of more complex tiltrotor geometries in future work.

## 6 CONCLUSIONS

The CFD solver HMB 2.0 has been successfully applied by AgustaWestland to simulate the aerodynamic performance of tiltrotor blades.

A close agreement with published tiltrotor hover test data was found despite the geometric approximation. The work indicates the validity and robustness of the approach in sufficiently capturing the hover wake-induced effects on rotor performance

Propeller mode simulations are shown to accurately predict the tiltrotor forward flight performance test data. The influence of the hub spinner on propeller performance has been highlighted and is significant.

The application and validation of a state-of-the-art overset ‘Chimera’ meshing approach is an important milestone prior to the study of more advanced topics.

The work has helped to further extend the HMB validation database beyond conventional helicopter rotors. Additional confidence in the suitability of the HMB methodology to develop tiltrotor designs has been gained.

## 7 FUTURE WORK

The fundamental steps presented here will lead to the CFD analysis of more complex interactional aerodynamics problems which are of particular interest to tiltrotor designs. The practical design information and high level of detail obtained with tools such as HMB will help AgustaWestland Engineers to develop the tiltrotor technology improvements of the future.

## 8 ACKNOWLEDGMENTS

The author gratefully acknowledges the hard-work and support of the staff of the AgustaWestland-University of Liverpool Advanced Rotorcraft Centre (AWLARC) and would like to thank K. Baverstock (AgustaWestland). This work is partially funded by the UK Aerodynamics Centre under the project ‘HiperTilt’ – a UK Technology Strategy Board (TSB)-sponsored AgustaWestland Research project.

## REFERENCES

- [1] Steijl, R., Barakos, G.N., and Badcock, K.J., “A Framework for CFD Analysis of Helicopter Rotors in Hover and Forward Flight”, *Int. J. Numer. Meth. Fluids*, 51:819–847, 2006
- [2] M.D. Maisel, D.J. Giulianetti, and D.C. Dugan, “The History of the XV-15 Tilt Rotor Research Aircraft: From Concept to Flight”, NASA SP-2000-4517, 2000
- [3] C. W. Acree, Jr., R. J. Peyran, and W. Johnson “Rotor Design Options for Improving XV-15 Whirl-Flutter Stability

- Margins”, NASA/TP–2004-212262, March 2004
- [4] Felker, F.F., Betzina, M.D., Signor, D.B., “Performance and Loads Data from a Hover Test of a Full-Scale XV-15 Rotor”, NASA Technical Memorandum 86833, 1985
- [5] Ladson, C.L., and Brooks, C.W., Jr., “Development of a Computer Program to Obtain Ordinates for NACA 6- and 6A-Series Airfoils,” NASA TM X-3069, Sept., 1974
- [6] R. Steijl and G.N. Barakos, “Sliding Mesh Algorithm for CFD Analysis of Helicopter Rotor-Fuselage Aerodynamics”, Int. J. Numer. Meth. Fluids, 58:527–549, 2008
- [7] Srinivasan, G R., Raghavan, V., Duque, E P N., “Flowfield Analysis of Modern Helicopter Rotors in Hover by Navier-Stokes Method”, Technical Specialists Meeting on Rotorcraft Acoustics and Rotor Fluid Dynamics, Philadelphia, PA, October 15-17, 1991
- [8] Menter, F.R., “Zonal Two Equation  $k-\omega$  Turbulence Models for Aerodynamic Flows”, AIAA 93-2906, 1993 / Menter, F.R., "Two-Equation eddy-viscosity turbulence models for engineering applications", AIAA, 32, 1598–1605, 1994.
- [9] Jeong, J., Hussain, F., “On the Identification of a Vortex”, Journal of Fluid Mechanics, Vol. 285, pp69-94, 1995
- [10] Kaul, U. K. & Ahmad, J., "Skin-Friction Predictions on a Hovering Tilt-Rotor Blade" Journal of Aircraft, 2012, Vol. 49, No.6
- [11] Betzina, M.D., “Rotor Performance of an Isolated Full-Scale XV-15 Tiltrotor in Helicopter Mode”, American Helicopter Society Aerodynamics, Acoustics, and Test and Evaluation Technical Specialists Meeting, San Francisco, CA, January 23-25, 2002
- [12] Light, J. S., “Results from an XV-15 Rotor Test in the National Full-Scale Aerodynamics Complex,” American Helicopter society 53rd Annual Forum, Virginia Beach, Virginia, April 1997
- [13] Farrell, M.K., “Aerodynamic Design of the V-22 Osprey Proprotor”, Presented at the 45<sup>th</sup> Annual Forum of the American Helicopter Society, Boston, MA, May 22-24, 1989
- [14] Johnson, W., “An Assessment of Capability To Calculate Tilting Prop-Rotor Aircraft Performance, Loads and Stability”, NASA TP-2291, March 1984
- [15] Anon, “Advancement of Proprotor Technology Task II – Wind Tunnel Results,” NASA CR114363, September 30, 1971
- [16] Johnson, W., Lau, B.H., Bowles, J.V., “Calculated Performance, Stability, and Maneuverability of High-Speed Tilting-Prop-Rotor Aircraft”, NASA TM-88349, September 1986
- [17] Jarkowski, M., Woodgate M., Rokicki J., and Barakos, G., “Towards Consistent Hybrid Overset Meshes for Rotorcraft CFD” Paper 099, Presented at the 37<sup>th</sup> European Rotorcraft Forum, Gallarate (Italy), September 13-15, 2011

r/R [ ]	Section [ ]
0.09	NACA 64-935
0.17	NACA 64-528
0.51	NACA 64-118
0.80	NACA 64-(1.5)12
1.00	NACA 64-208

Table 1 XV-15 rotor aerofoil radial positions and identities, [4]

$M_{TIP}$ [ ]	0.69
$Re_{TIP}$ [ ]	5E+05
$\theta_{75}$ [°]	3,6,10,13

Table 2 XV-15 hover simulated conditions

$M_{TIP}$ [ ]	0.54
$Re_{TIP}$ [ ]	4.5E+05

Table 3 XV-15 propeller simulated conditions

$\theta_{75}$ [°]	$C_T$ [ ]	$C_o$ [ ]	FoM [ ]
3	0.002970	0.000239	0.480
6	0.005260	0.000402	0.670
10	0.009085	0.000798	0.768
13	0.012261	0.001255	0.765

Table 4 XV-15 HMB  $k-\omega$  SST hover total force and FoM predictions

Advance ratio [ ]	$C_T$ [ ]	$C_o$ [ ]	$\eta$ [ ]
<i>Low</i>	0.001728	0.000671	0.870
	0.003144	0.001183	0.898
	0.004555	0.001705	0.902
	0.005680	0.002132	0.900
<i>Moderate</i>	0.001153	0.000716	0.816
	0.002799	0.001570	0.904
	0.003455	0.001915	0.914

Table 5 XV-15 HMB  $k-\omega$  SST propeller total force and propulsive efficiency predictions (excl. spinner)

	$\Delta C_T$ [ ]	$\Delta C_o$ [ ]	$\Delta \text{FoM}$ [ ]
Variation	0.000126	0.000012	0.002159
Variation as percentage	0.69%	0.76%	0.28%

Table 6 XV-15 HMB hover variation in total force and FoM predictions between results obtained using baseline and Chimera meshes



Figure 1 XV-15 in low-level hover mode flight (NASA photo)

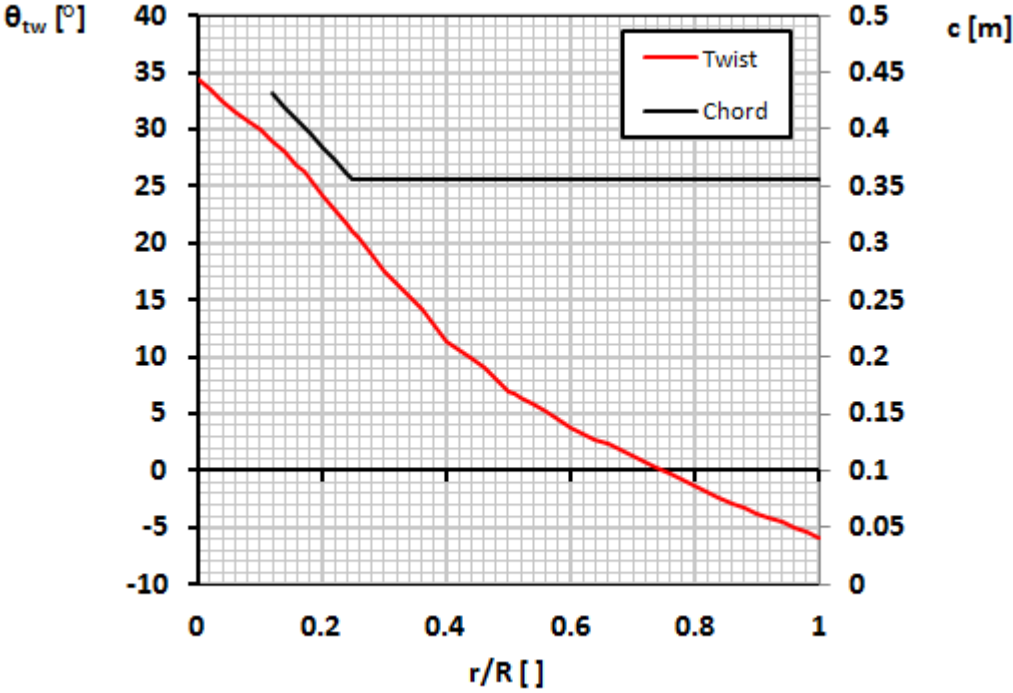


Figure 2 XV-15 blade radial twist & chord distributions, [3]

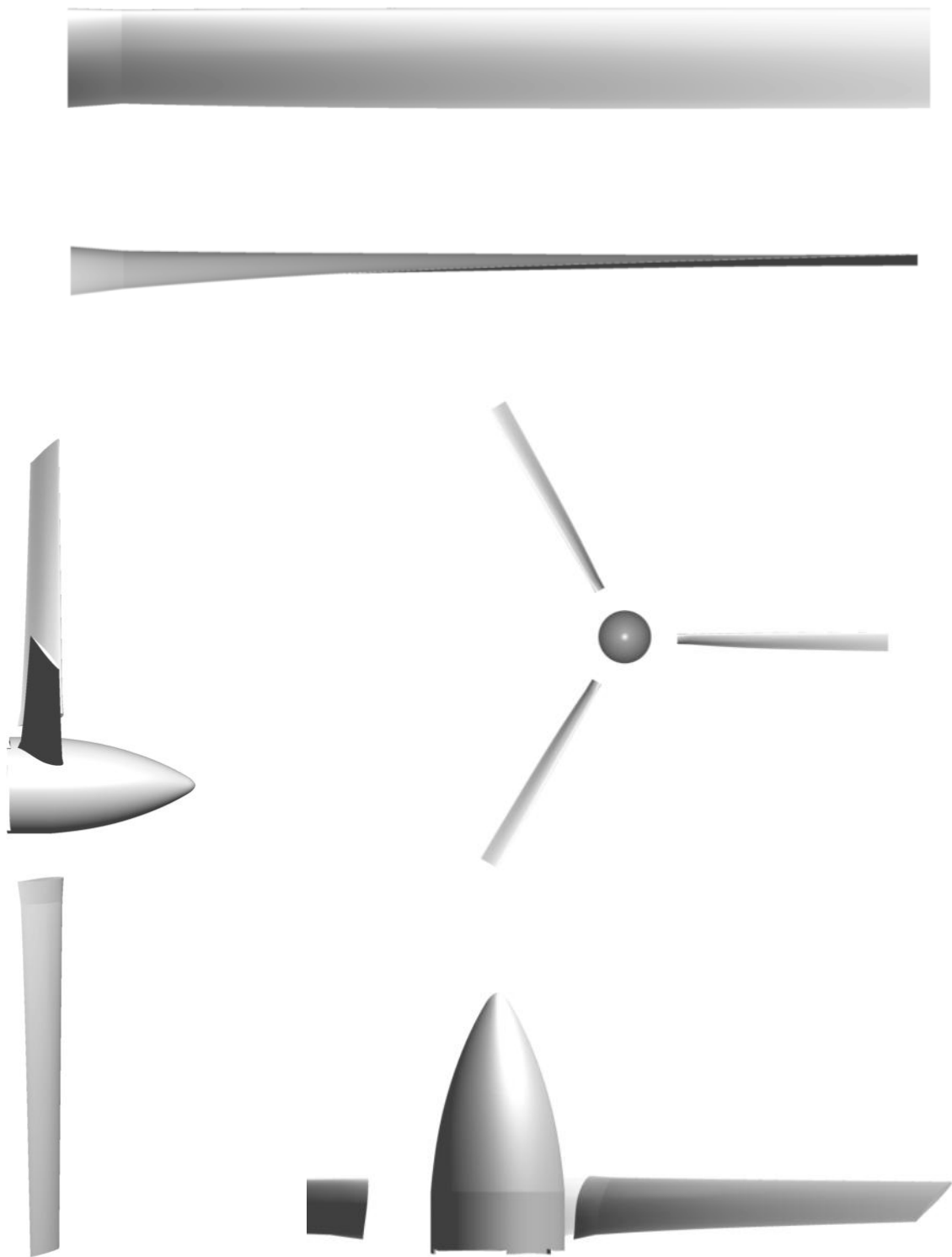


Figure 3 XV-15 rotor geometry reconstruction

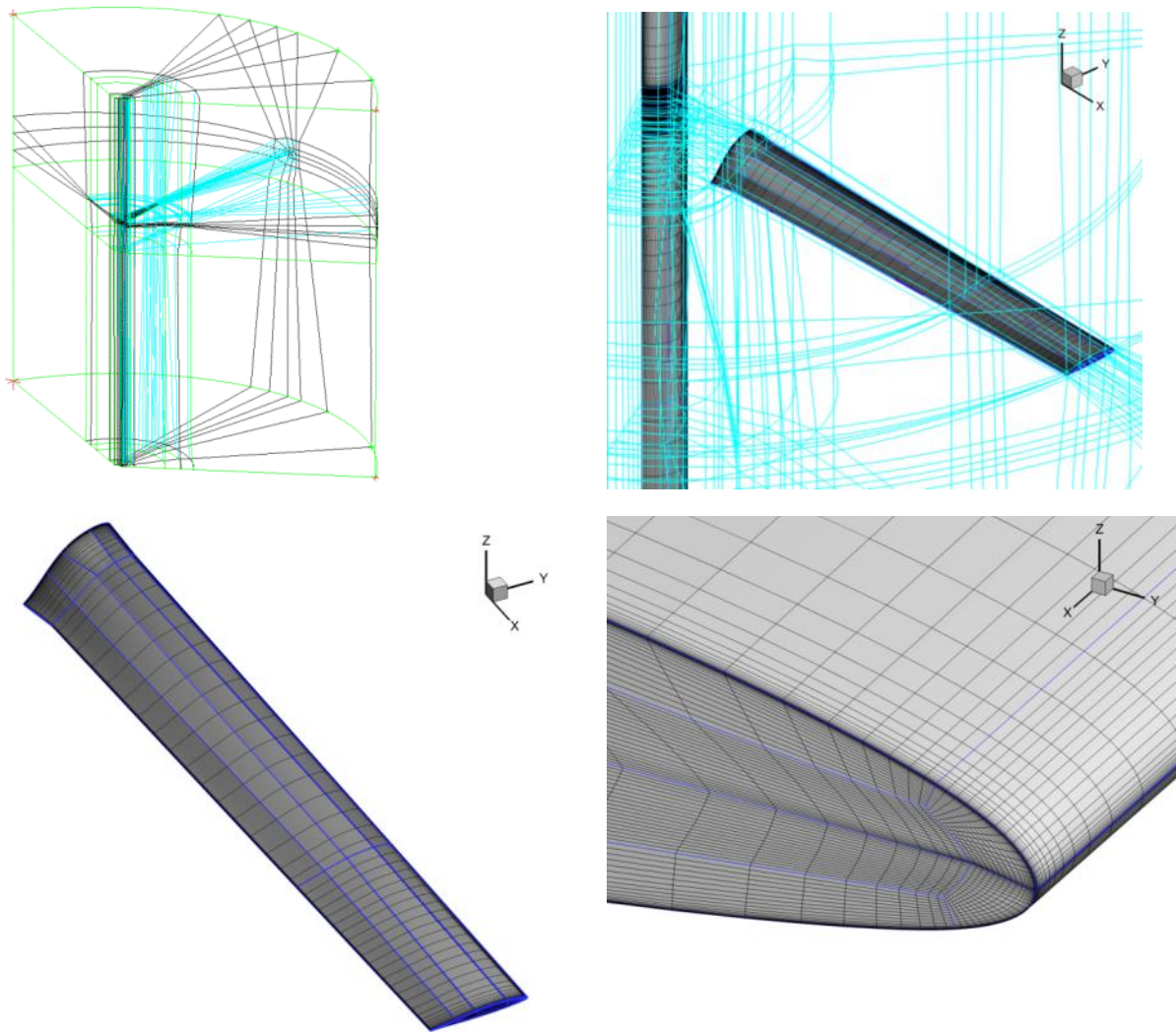


Figure 4 XV-15 HMB structured multi-block mesh domain, topology and surface mesh detail, hover

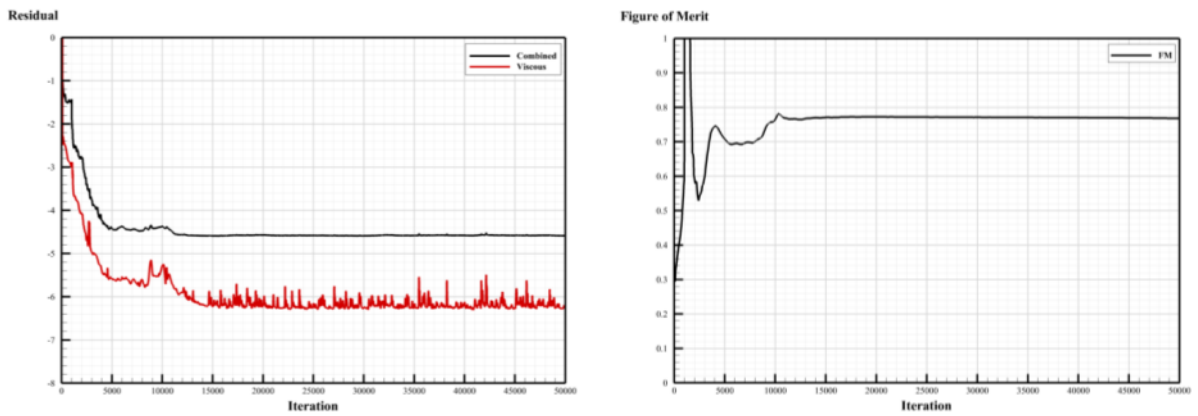


Figure 5 Sample HMB convergence history; calculation residuals and predicted rotor FoM, hover  $\theta_{75} = 10^\circ$ .

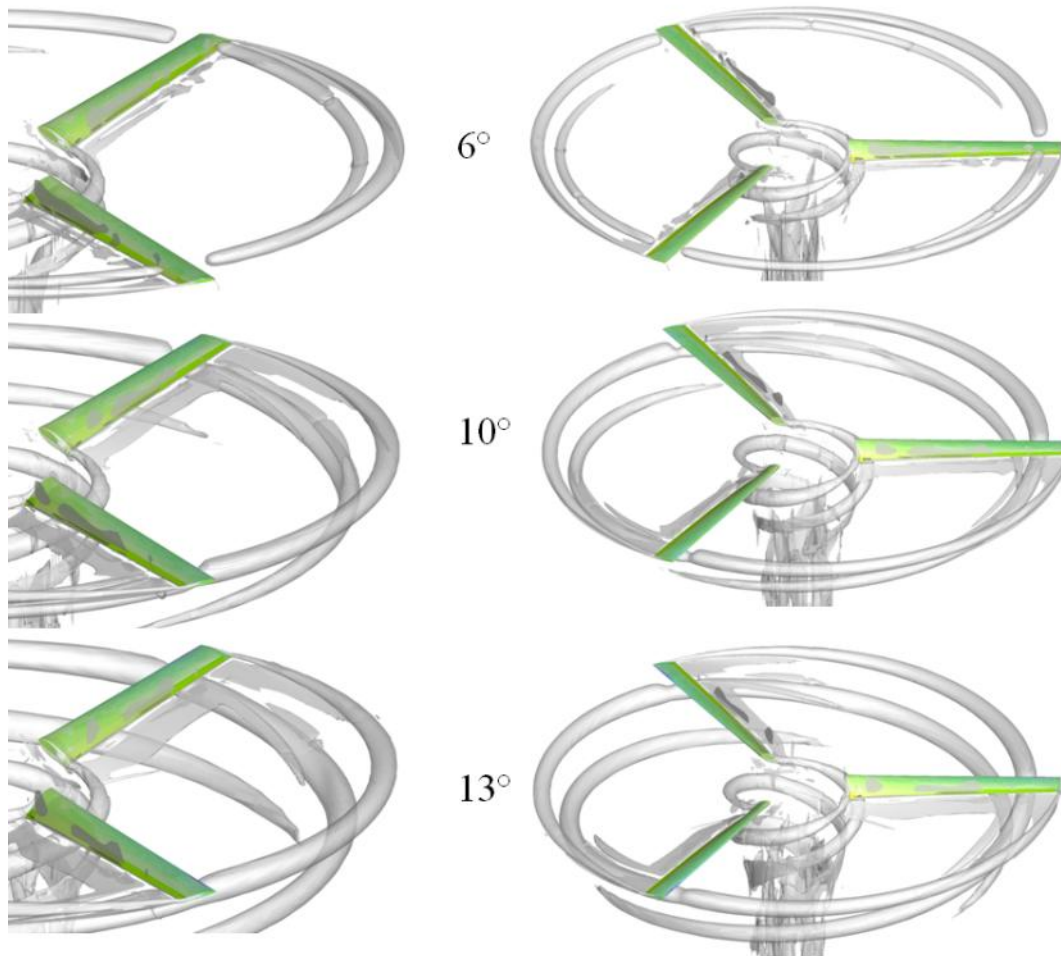


Figure 6 XV-15 HMB predicted hover wake variation with collective pitch, iso-surfaces of  $Q=0.01$

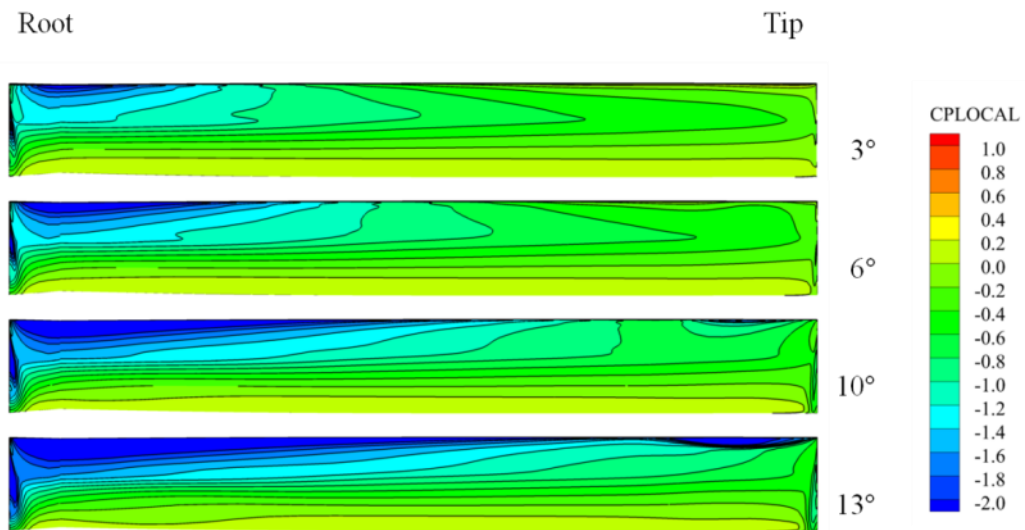


Figure 7 XV-15 HMB hover blade upper surface pressure coefficient predictions with collective pitch

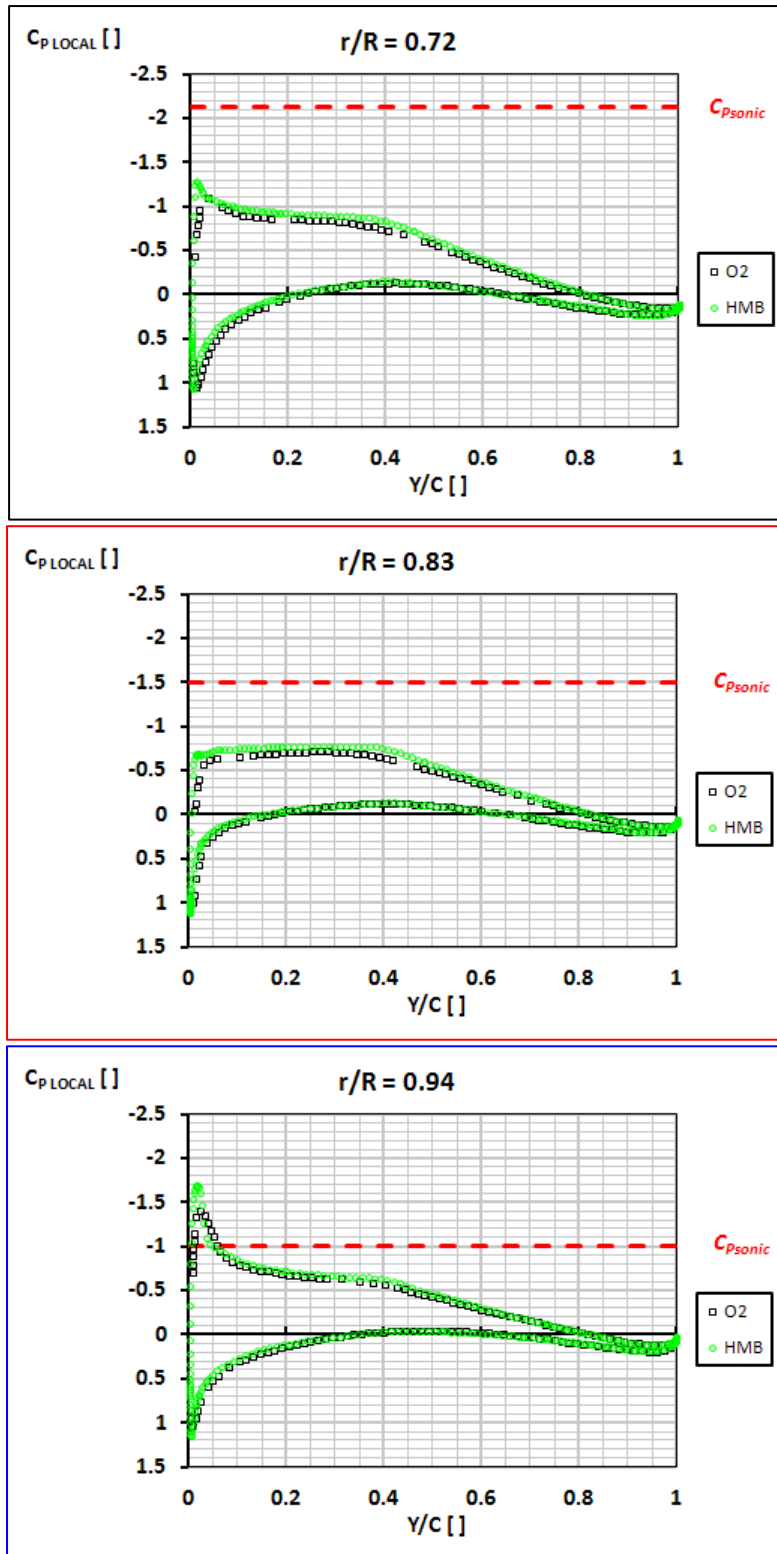
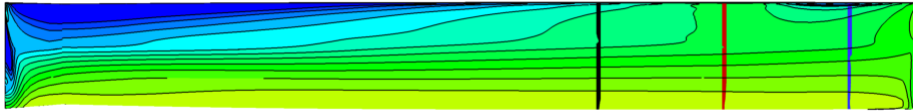


Figure 8 XV-15 HMB  $k-\omega$  SST hover predicted chordwise pressure distributions for three radial stations compared with OVERFLOW2 (O2) SA predictions from [10],  $\theta_{75} = 10^\circ$

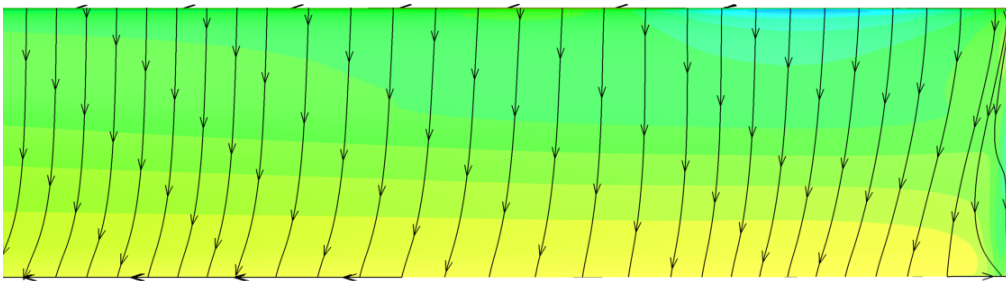


10°

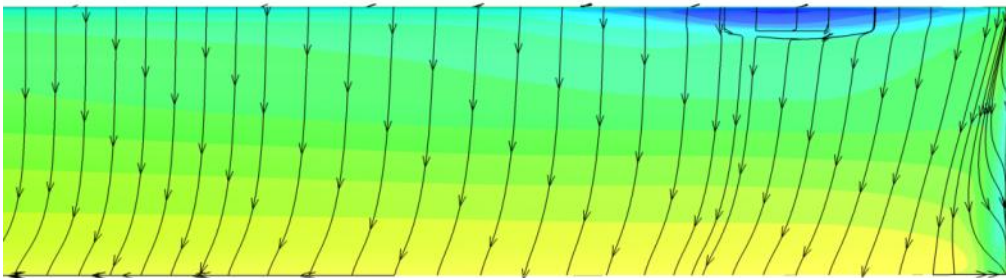


13°

Figure 9 XV-15 HMB hover predicted supercritical region at  $\theta_{75} = 10$  &  $13^\circ$



10°



13°

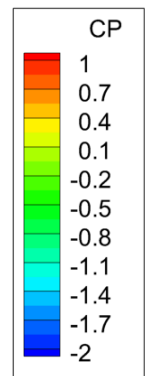


Figure 10 XV-15 HMB hover predicted surface streamlines at  $\theta_{75} = 10$  &  $13^\circ$

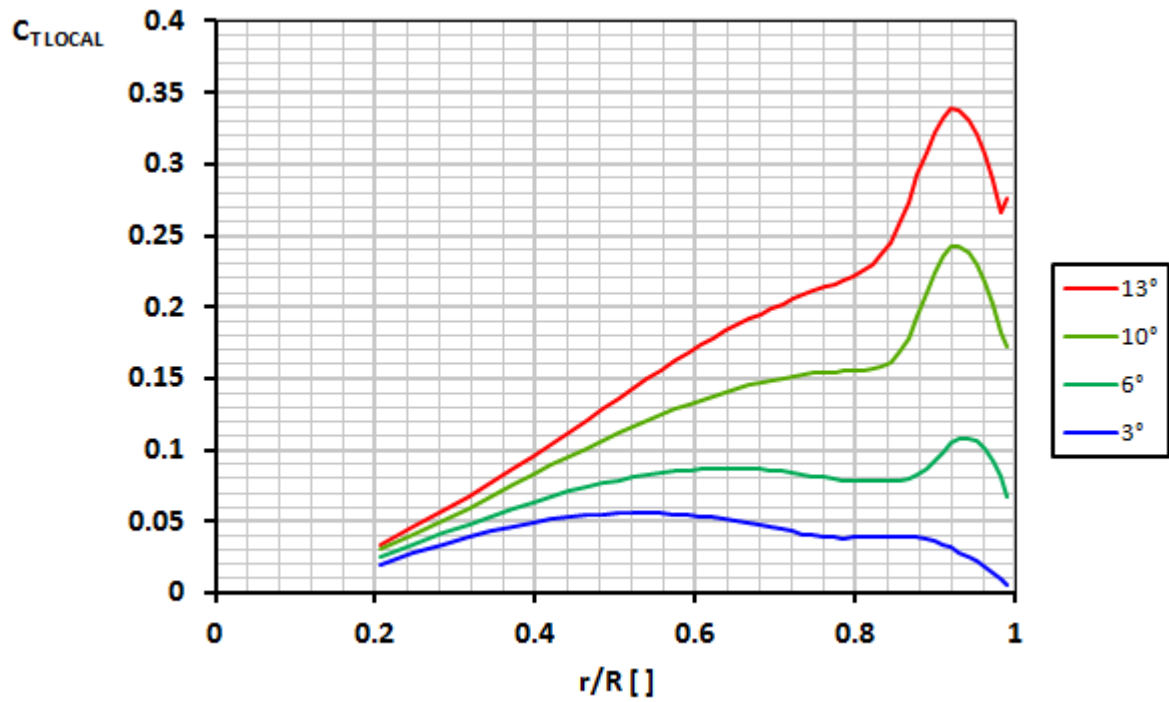


Figure 11 XV-15 HMB hover predicted radial thrust distribution variation with collective pitch

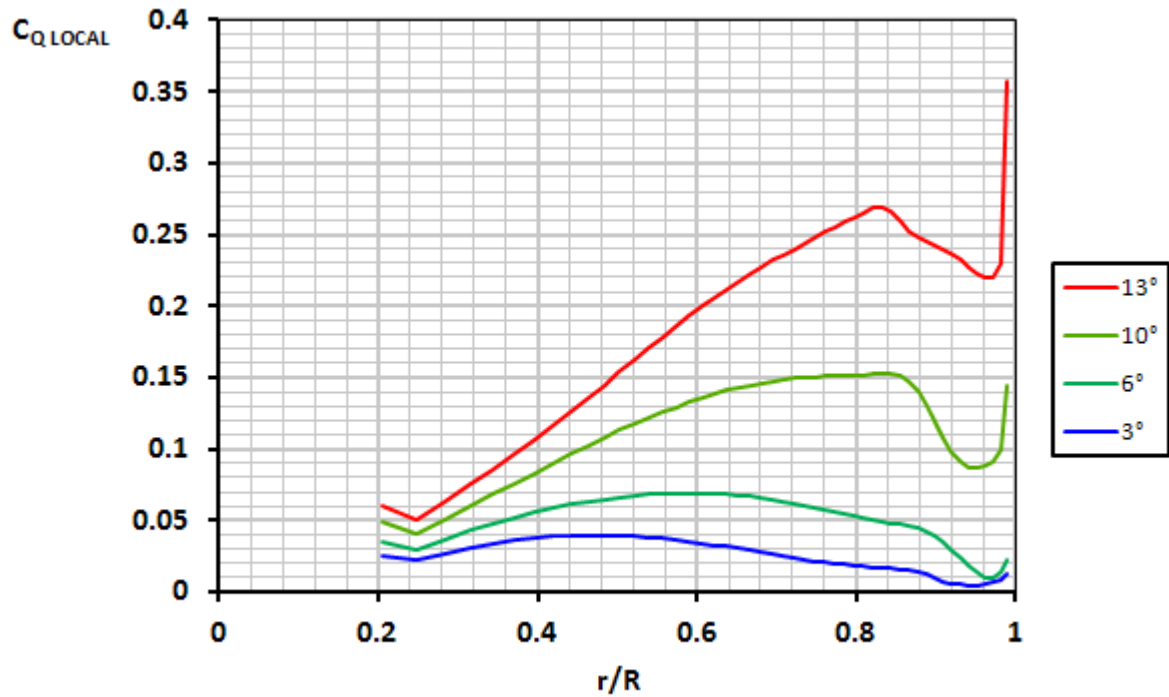


Figure 12 XV-15 HMB hover predicted radial torque distribution variation with collective pitch

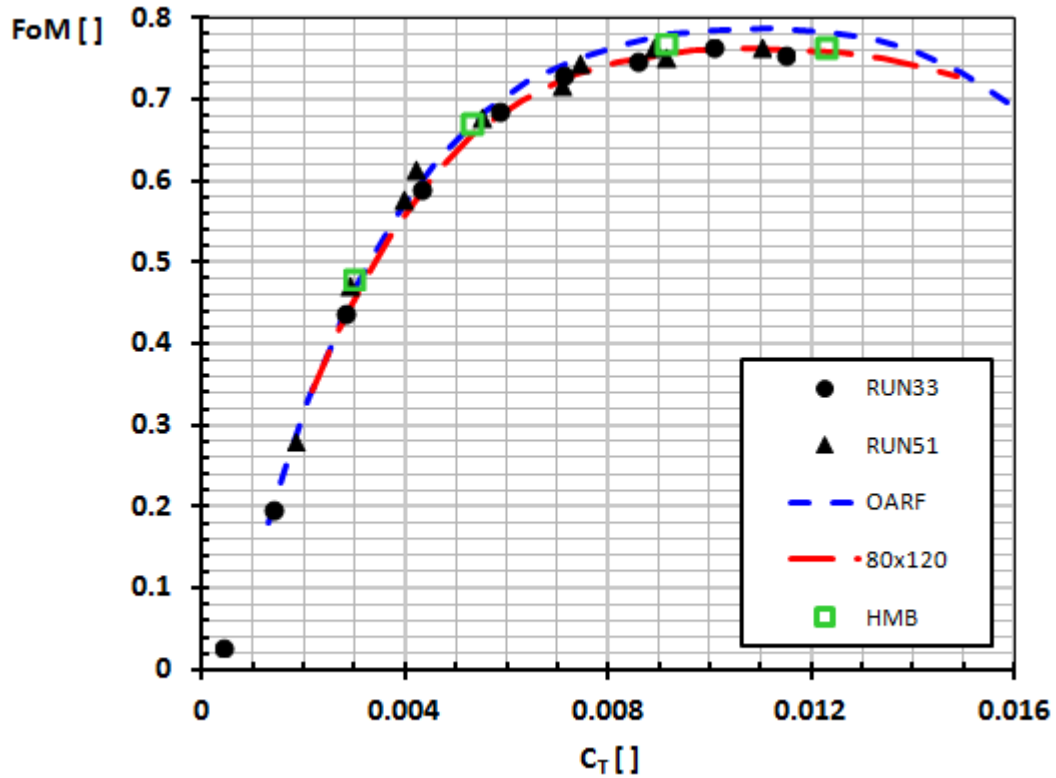


Figure 13 XV-15 HMB hover predicted rotor FoM variation with thrust coefficient vs. experimental measurements (OARF [4], 80x120 [12] and runs 33&51 [11])

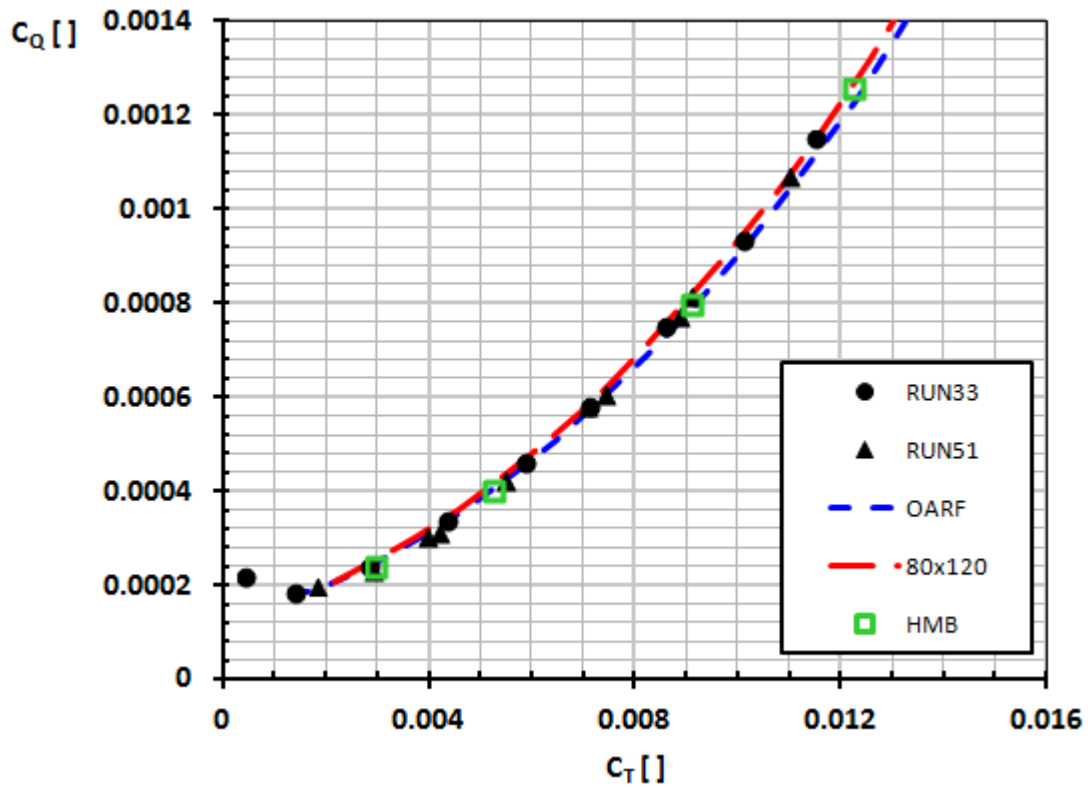


Figure 14 XV-15 HMB hover predicted rotor torque coefficient variation with thrust coefficient vs. experimental measurements (OARF [4], 80x120 [12] and runs 33&51 [11])

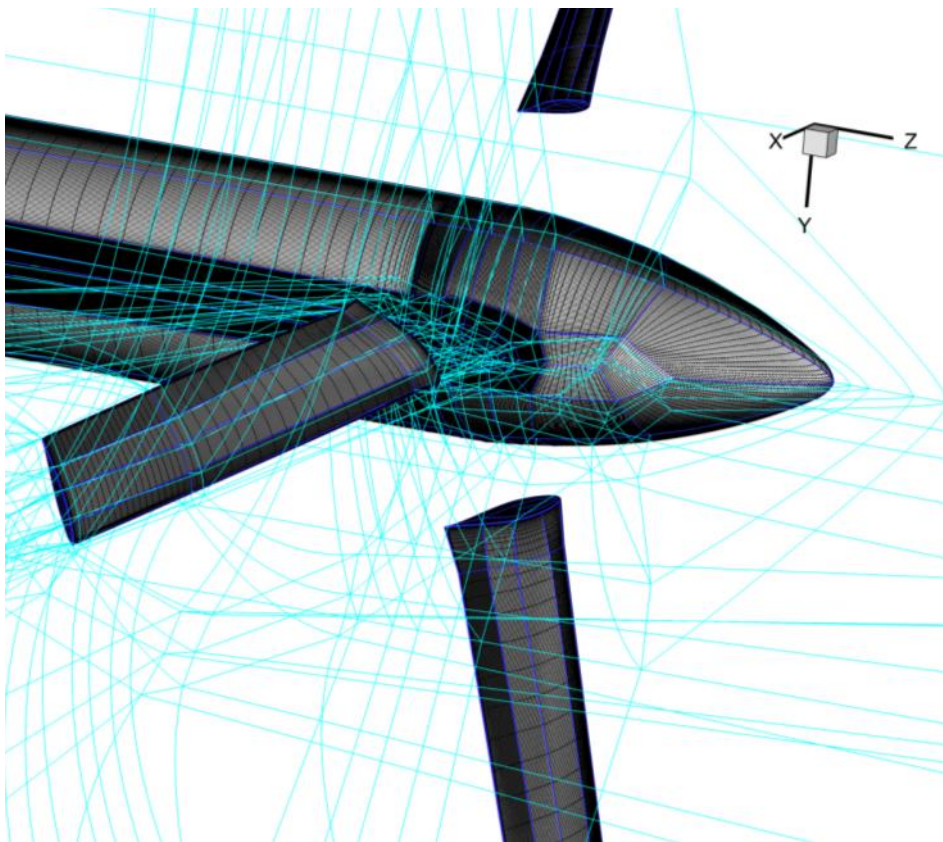
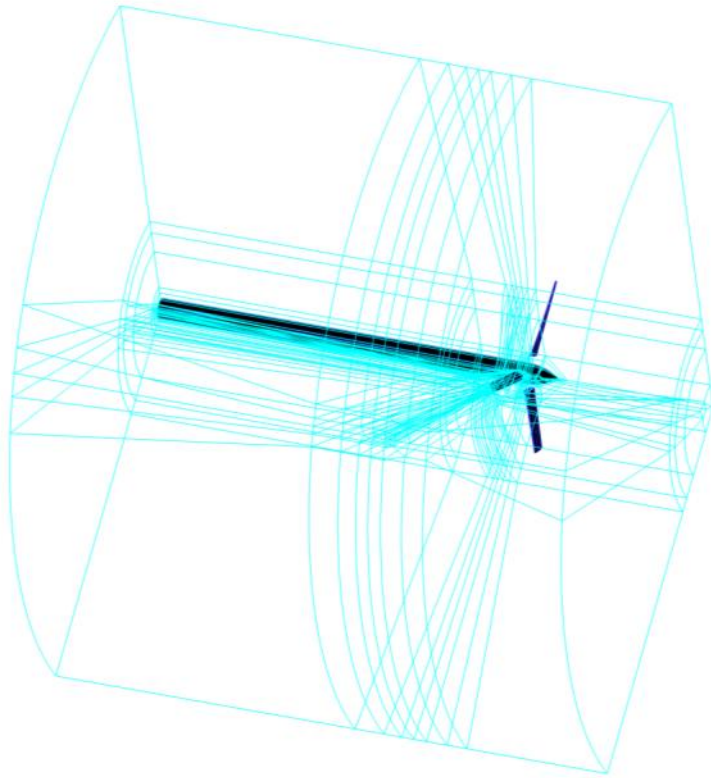
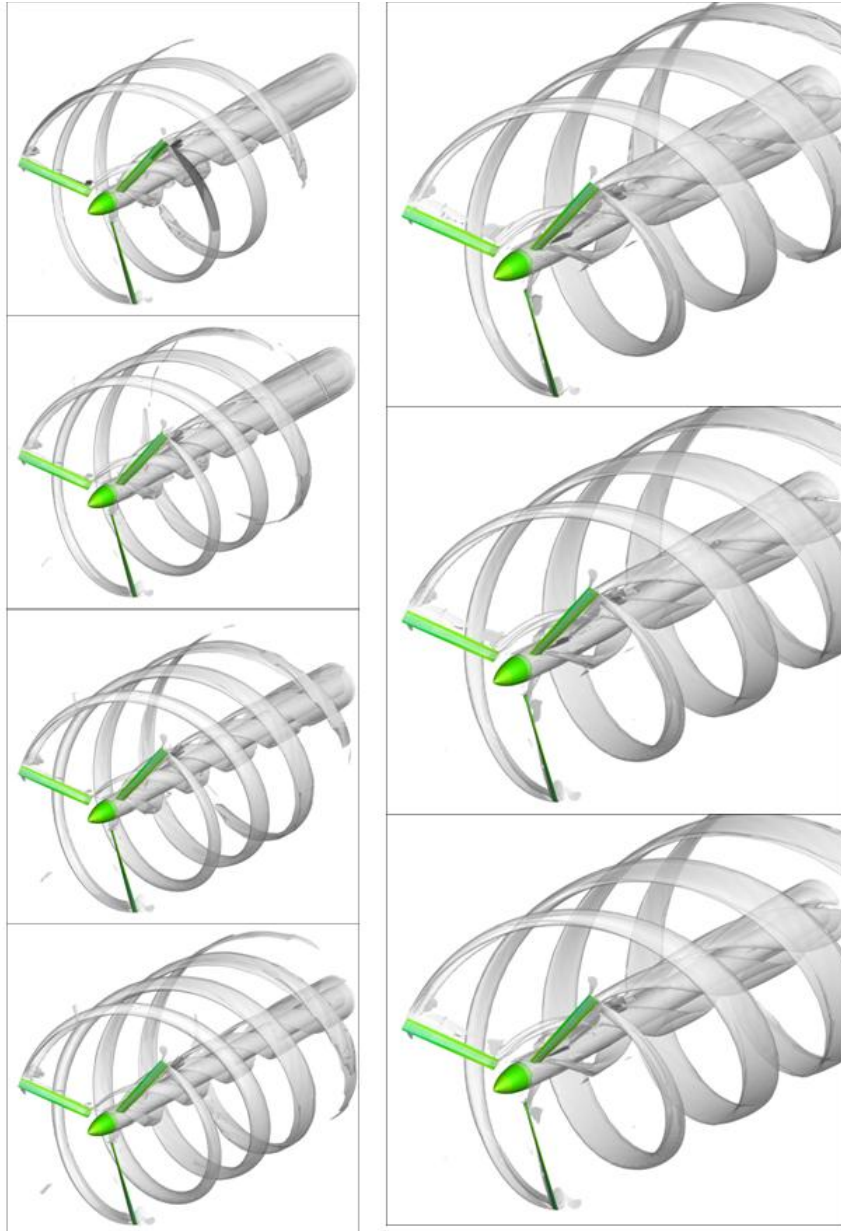
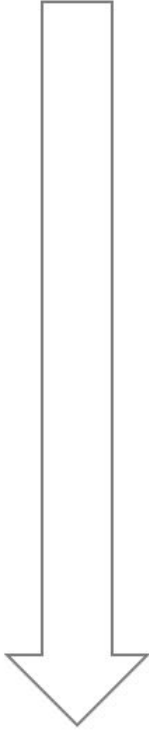


Figure 15 XV-15 HMB structured multi-block mesh domain showing blocking topology and surface mesh detail, propeller

Increasing  $\theta_{75}$



Low advance ratio

Moderate advance ratio

Figure 16 XV-15 HMB predicted propeller wake variation with collective pitch for a low and moderate advance ratio, iso-surfaces of  $Q=0.01$

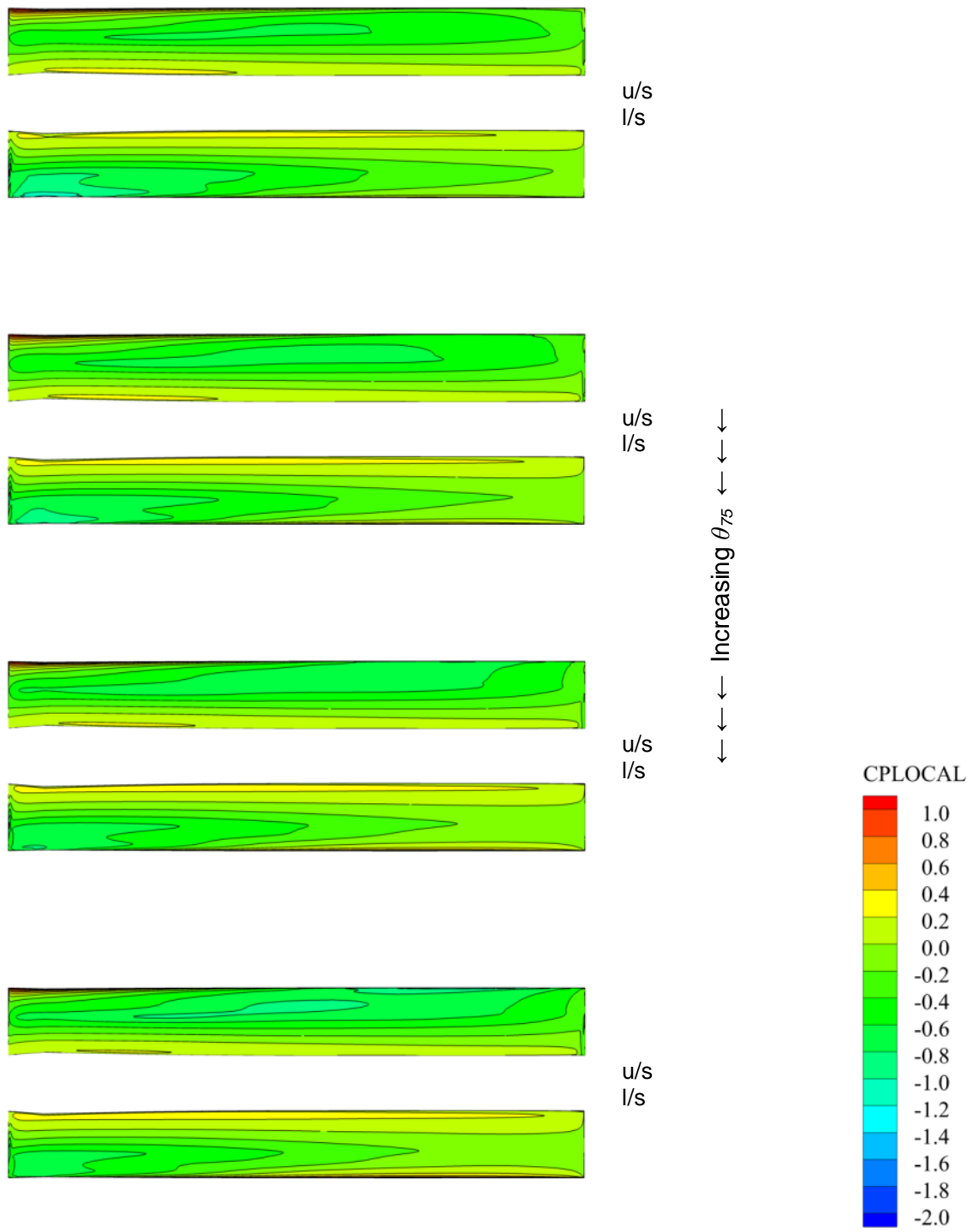


Figure 17 XV-15 HMB propeller blade upper & lower surface pressure coefficient predictions with collective pitch, low advance ratio

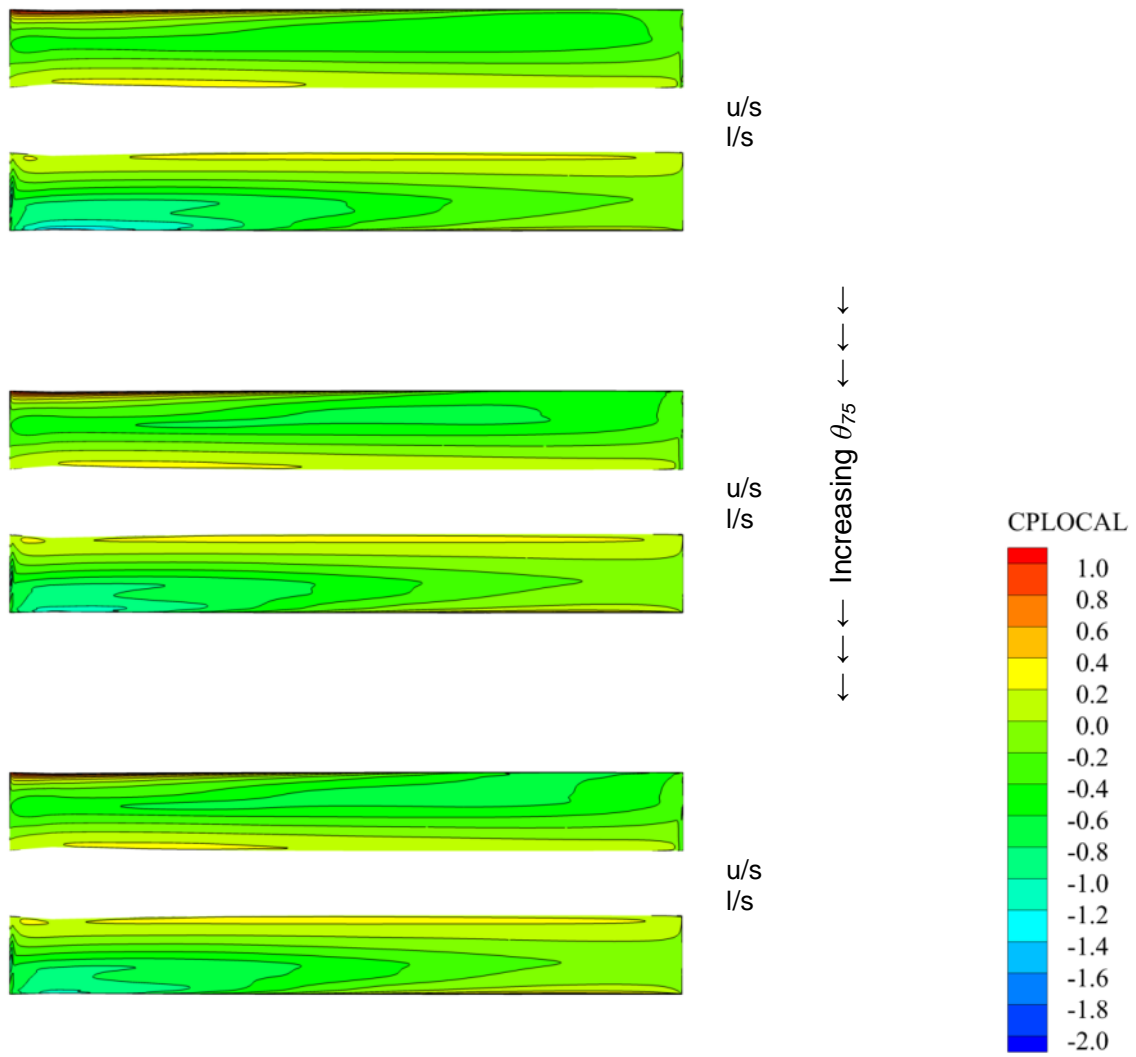


Figure 18 XV-15 HMB propeller blade upper & lower surface pressure coefficient predictions with collective pitch, moderate advance ratio

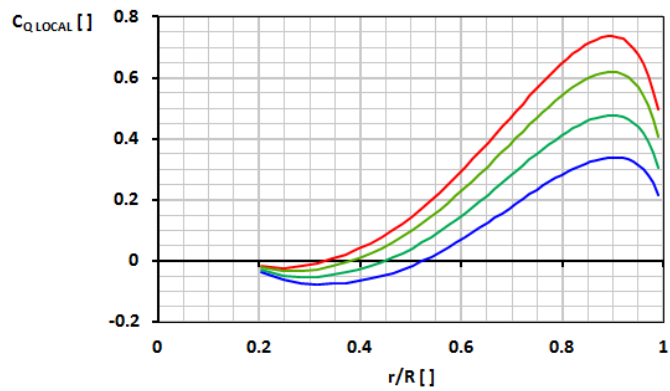
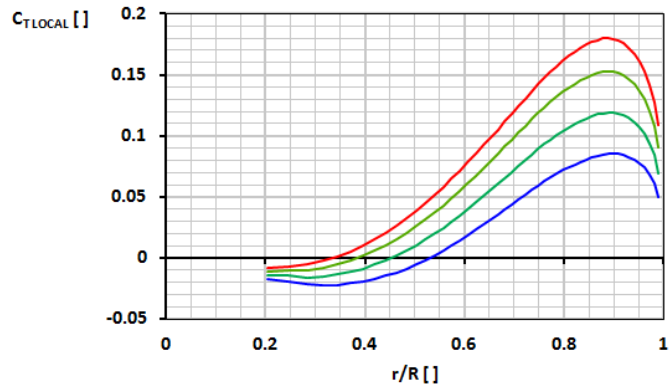


Figure 19 XV-15 HMB predicted propeller radial thrust & torque distribution variation with collective pitch, low advance ratio

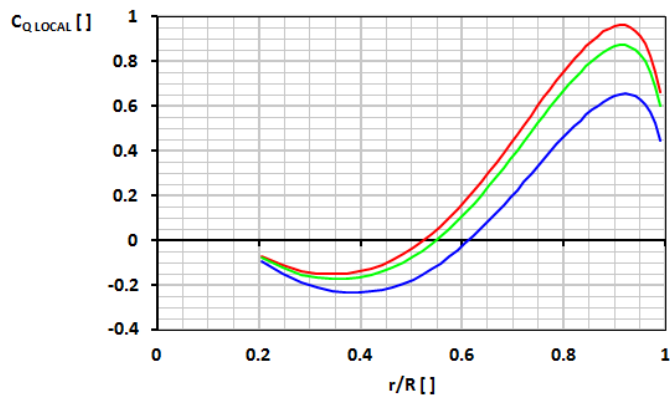
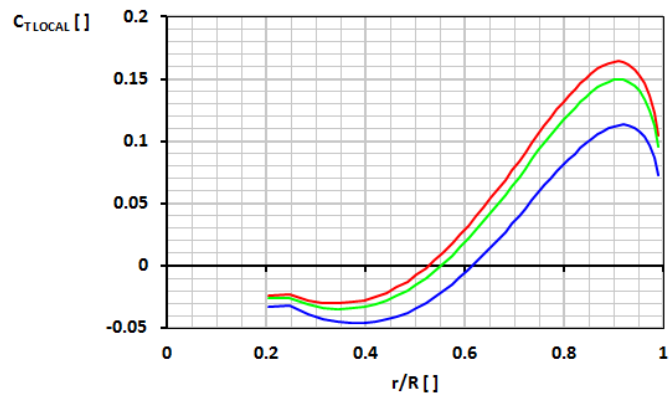
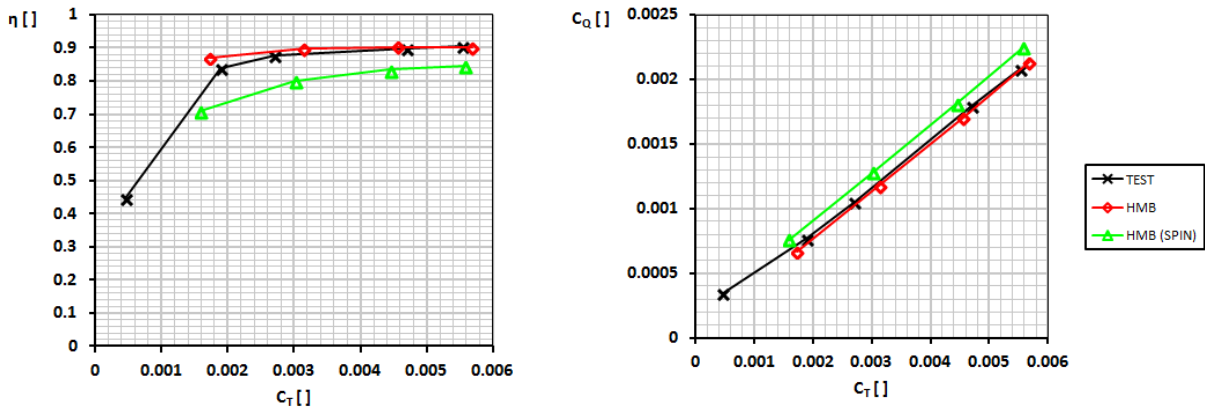
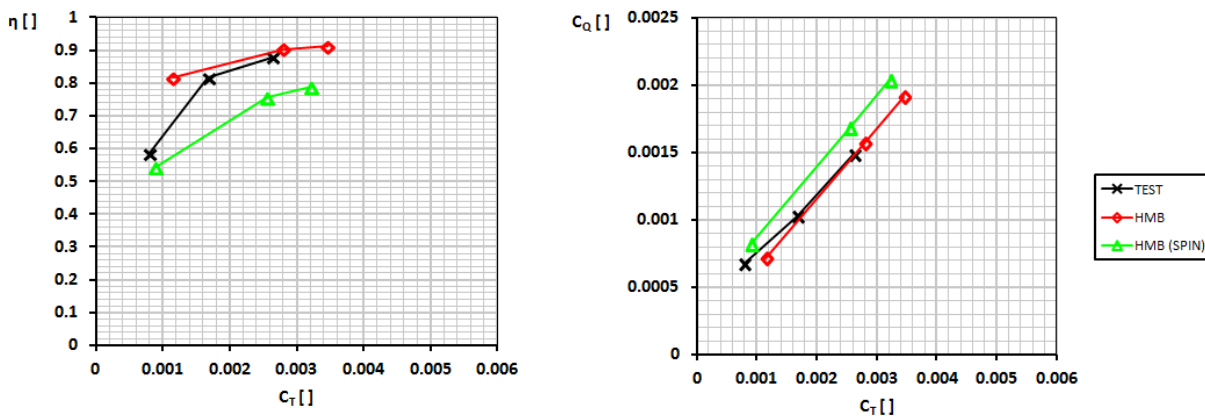


Figure 20 XV-15 HMB predicted propeller radial thrust & torque distribution variation with collective pitch, moderate advance ratio



*Low advance ratio*



*Moderate advance ratio*

Figure 21 XV-15 HMB predicted propeller propulsive efficiency, thrust & torque variation with collective pitch for two advance ratios vs. test data, [13]&[15] and including the spinner contribution (SPIN)

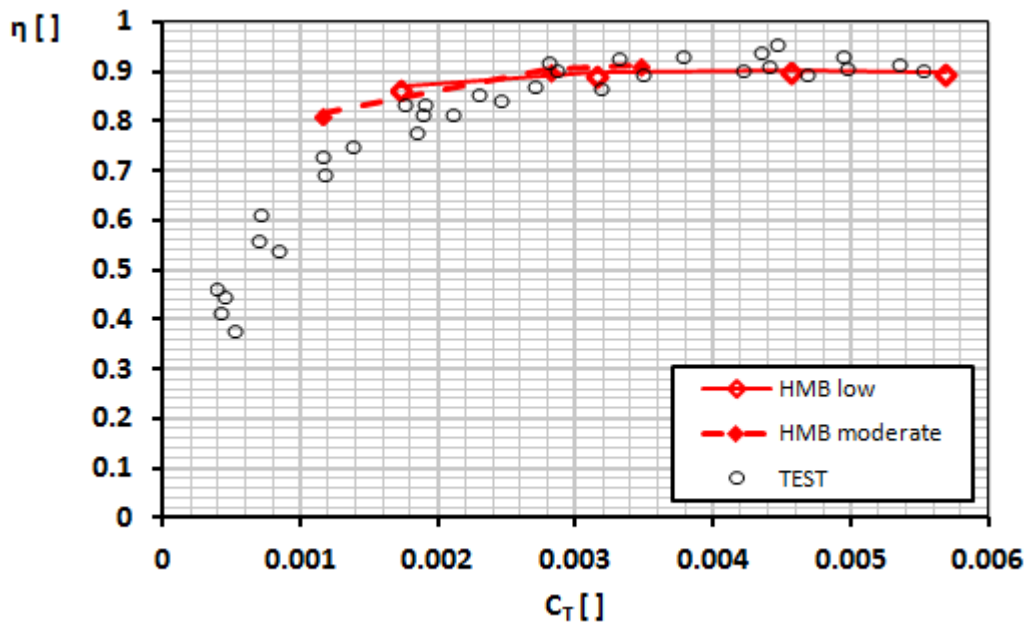


Figure 22 XV-15 HMB predicted propeller propulsive efficiency, thrust & torque variation with collective pitch for low and moderate advance ratios vs. test scatter (for various advance ratios), [16]

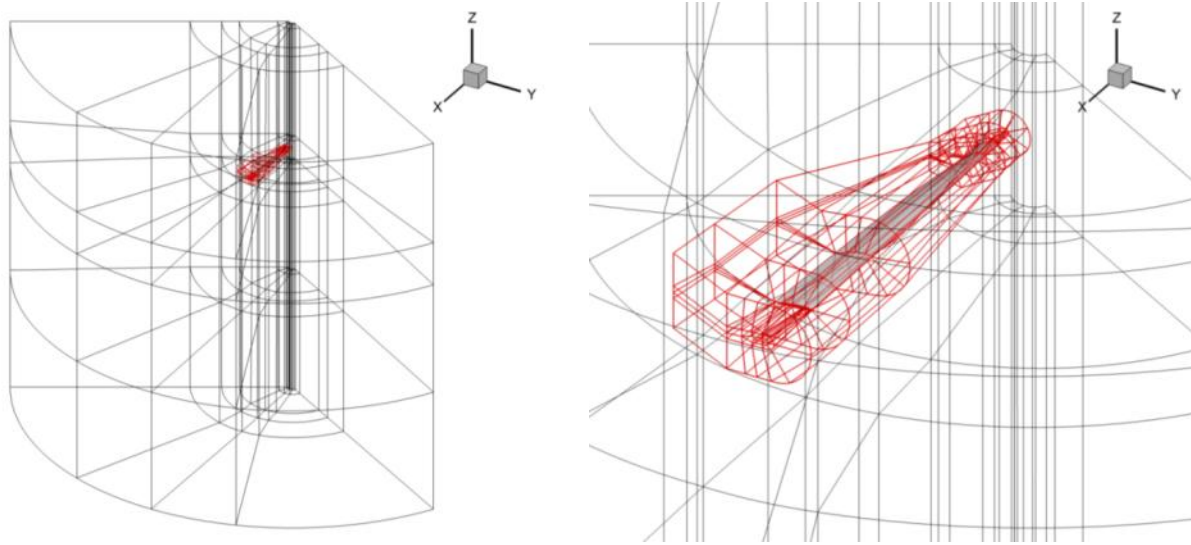


Figure 23 XV-15 HMB Chimera multi-block mesh topologies (blade foreground mesh in red, domain background mesh in black)

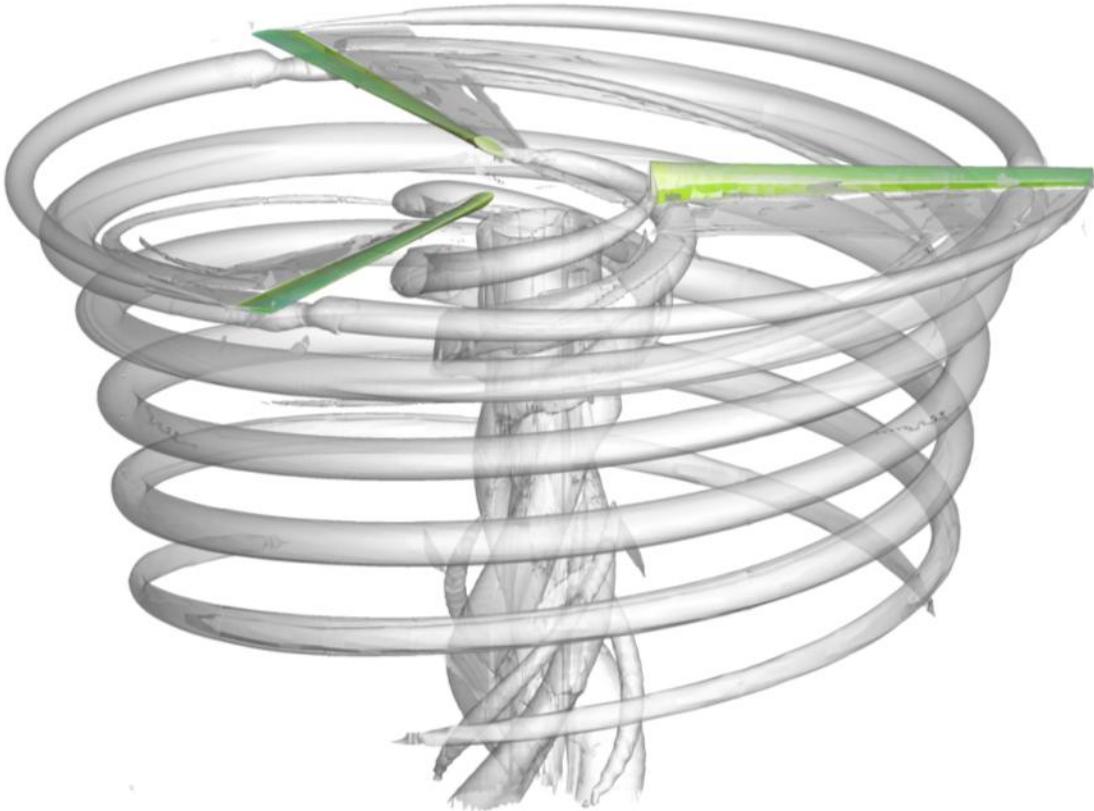


Figure 24 XV-15 HMB Chimera predicted hover  $\theta_7=10^\circ$  wake, iso-surfaces of  $Q=0.001$

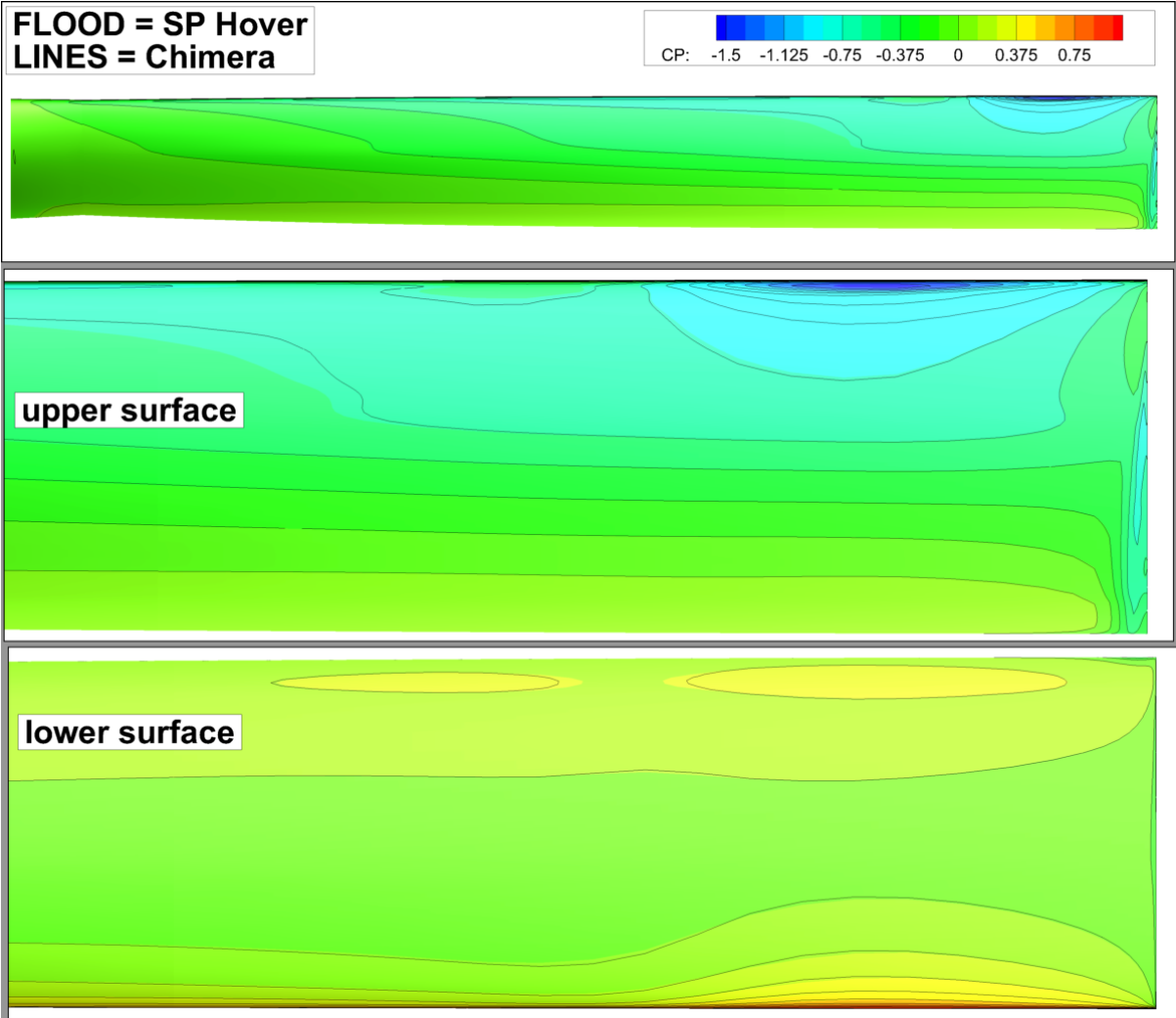


Figure 25 XV-15 HMB hover blade upper & lower surface pressure coefficient contours: Chimera mesh vs. baseline sliding planes (SP) mesh results

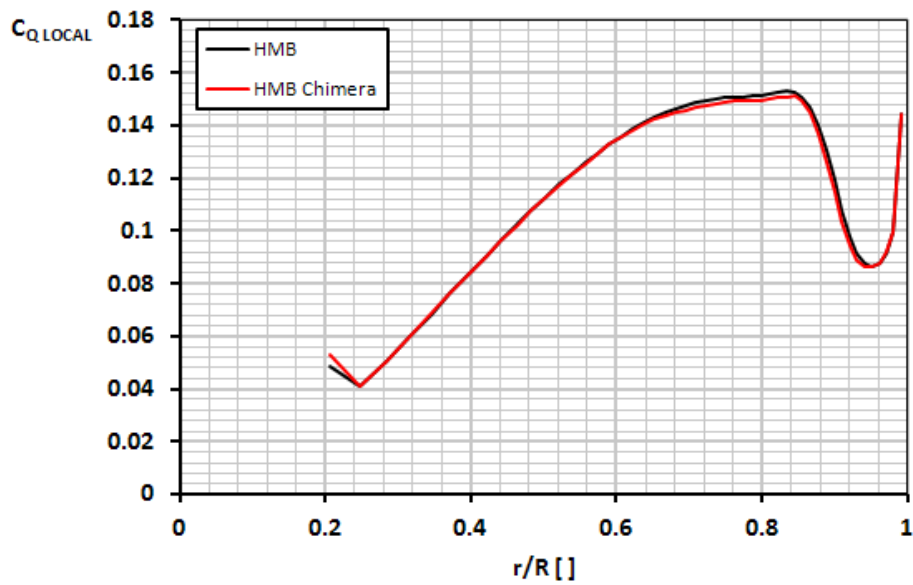
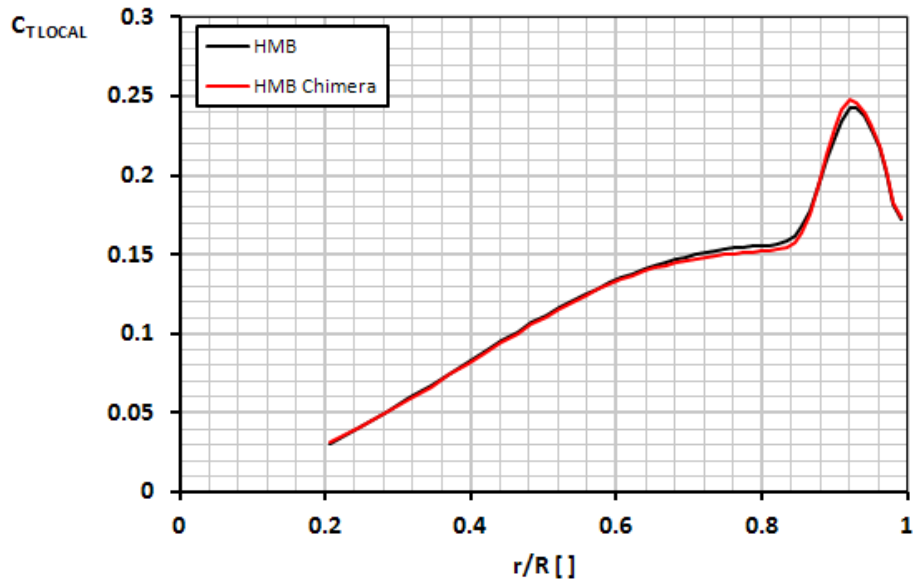


Figure 26 XV-15 HMB hover predicted radial thrust & torque distributions,  $\theta_{75}=10^\circ$ : Chimera vs. baseline mesh

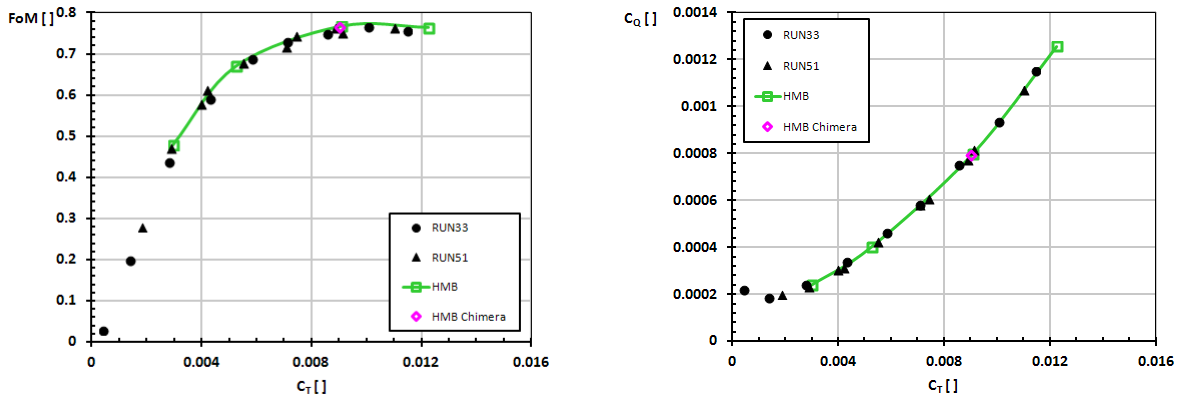


Figure 27 XV-15 HMB hover predicted FoM, thrust & torque,  $\theta_{75}=10^\circ$ : Chimera vs. baseline mesh with test data, [11]